



6X Acuros algorithm validation in the presence of inhomogeneities for VMAT treatment planning

Sarah Bassi*, Elaine Tyner

St.Luke's Hospital, Highfield Rd, Rathfarnham, Dublin 6, Ireland

ARTICLE INFO

Article history:

Received 8 November 2019
Received in revised form 17 January 2020
Accepted 25 March 2020
Available online 29 April 2020

Keywords:

Acuros®XB (AXB) version 13.7 algorithm
Anisotropic Analytic Algorithm
GafChromic® EBT2
MapCheck measurements
VMAT treatment plans.

ABSTRACT

Aim: To validate the Acuros®XB (AXB) dose calculation algorithm for a 6MV beam from the Varian TrueBeam treatment units.

Background: Currently Anisotropic Analytic Algorithm (AAA) is clinically used on authors' department but AXB could replace it for VMAT treatments in regions where inhomogeneities and free air are present. **Materials and methods:** Two steps are followed in the validation process of a new dose calculation algorithm. The first is to check the accuracy of algorithm for a homogenous phantom and regular fields. Multiple fields of increasing complexity have been acquired using a MapCheck diode array. The accuracy of the algorithm was evaluated using the gamma analysis method. The second is to validate the algorithm in the presence of heterogeneous media. Planar absolute dose was measured with GafChromic®EBT2 film and was compared with the dose calculated by AXB. Gamma analysis was performed between MapCheck measurements and AXB dose calculations, at a range of clinical source-surface distance.

Results: For SSDs ranging from 80 to 100 cm, the results show a minimum pass rate of 95% between AXB and MapCheck acquisition. For open 6MV photon beam interacting with a phantom with an air gap, the agreement after the air gap between AXB and GafChromic®EBT2 is less than 1% in the $3 \times 3\text{cm}^2$ field and less than 2% in the $10 \times 10\text{cm}^2$ field.

Conclusions: AXB has advanced modelling of lateral electron transport that enables a more accurate dose calculation in heterogeneous regions and, compared with AAA, improves accuracy between different density interfaces. This will be of particular benefit for head/neck treatments.

© 2020 Greater Poland Cancer Centre. Published by Elsevier B.V. All rights reserved.

1. Background

Dose calculation algorithms play a crucial role in modern treatment planning systems (TPS). With the advent of intensity-modulated radiation therapy (IMRT) the previous ICRU recommendation of 5% absorbed-dose accuracy is replaced by a statistical measure. In high gradient situations (more than 20%/cm) the use of distance to agreement (DTA) with an accuracy of 3.5 mm is recommended. While in low gradient regions, the difference between the measured (or independently computed) absorbed dose and the treatment-planning absorbed dose, normalized to the absorbed-dose prescription should be no more than 3.5%.² This implies that each step (machine calibration, patient positioning, dose calculation, target and organs at risk delineation, etc.) needs to be performed to accuracy better than 5%. The necessary accuracy for the dose calculation step should be in the order of 2–3% in dose and 2–3 mm of DTA.^{3,4}

Semi-analytical algorithms for dose calculations of photons beams like pencil beam convolution algorithms, Anisotropic Analytical Algorithm (AAA) or superposition/convolution algorithms are known for their limited accuracy in regions of large inhomogeneities.^{5,6} Acuros®XB Advanced Dose Calculation (AXB in the following) has been implemented in the Eclipse treatment planning system (Varian Medical Systems, Palo Alto, USA). The AXB algorithm explicitly models the physical interaction of radiation with matter [M1] and for this feature the dose deposition in regions of large inhomogeneities is well estimated. Compared to Monte Carlo (MC), the golden standard for dose calculation, several validation studies^{7,9,10} have shown a good agreement with the AXB algorithm in regions of large inhomogeneity.

Before presenting the methods and materials, it would be helpful to first give a panoramic of the types of algorithms involved in this work.

The classification of an algorithm can be made using different criteria. One of the most common classifications was proposed by Ojala et al.¹¹ that classified the algorithms taking into consideration how they model the lateral electron transport. "Type A" algorithms

* Corresponding author.

don't model the changes in lateral transport. These algorithms rely on measurements in water and apply simplified corrections for patient contour and heterogeneities. These are pencil beam algorithms. In "type B" algorithms various approximate methods are used to model lateral electron transport. AAA, CCC, fast MC are type B algorithms.

AAA is a 3D pencil beam convolution/superposition algorithm. The basic physical parameters used to characterize the fluence and energy spectra of the photons and electrons present in the clinical beam and their fundamental scattering properties in water equivalent medium are pre-calculated by MC. During the beam data configuration phase, these basic physical parameters are modified to match the actual measured clinical beam data, acquired in a water tank with an ionisation chamber. This gives a model of the fluence and energy spectrum from the head of the linear accelerator. The physical parameters, which are specific for the treatment unit, are stored as a phase space file and later retrieved for actual dose calculation. The broad clinical beam is divided into finite-size beamlets. From MC calculation, the photon beam attenuation as energy deposition density function $I\beta(z,\rho)$ and the photon scatter as scatter kernel $K\beta(x,y,z,\rho)$ that defines the lateral dose scattering are known for each beamlet. The photon component is separate from electron one. The algorithm does not account for chemical material/tissue properties; hence, scatter kernels and their depth dependencies are determined at the time of configuration for a water-equivalent medium. In heterogeneous media the kernels and depth dependencies are rescaled according to the specific density. The dose calculation is based on the convolutions over the beamlet cross-sections (that corresponds to the resolution of the calculation voxel) separately for the primary photons, extra-focal photons (second source), and for electrons contaminating the primary beam. The dose distribution resulting from an arbitrary beamlet is calculated by the convolution of photon fluence (assumed to be uniform over the small cross-section of a beamlet), $I\beta(z,\rho)$ and $K\beta(x,y,z,\rho)$ functions. The final dose is obtained by a superposition of the separate dose contributions from the primary photons, extra-focal photons, and contaminating electrons from all individual beamlets [M2].

Full MC and AXB are "Type C" algorithms because they have an advance modelling of lateral electron transport and are grid-based Linear Boltzmann Transport Equation (LBTE) solvers. These algorithms calculate the dose deposition also in the presence of high-Z implanted materials. The dose is reported as dose-to-medium. AXB explicitly solves the LBTE by numerical methods. The algorithm discretizes in space, angle and energy and solves the equation in a particular range of energy, space and angle. The disadvantage of discretization is that it can produce systematic errors. MC indirectly obtains the solution of LBTE by following a large number of particle transports through successive random sampling in media and the simulation of a finite number of particles can produce stochastic errors. In contrast to AAA where density scaling of the kernels occurs, AXB uses the chemical composition of the medium in each dose calculation voxel. From the CT calibration curve, the Hounsfield Unit (HU) is converted in the mass density values for each voxel. A hard coded look-up table stored in the Varian system database is used to convert the mass density value, which is derived from the CT HU to mass density calibration curve, to a material composition for a given voxel in the CT scan. In AXB version 13.7 this table is composed of 22 material types, ranging from air to stainless steel with 5 biological material types. This is more than the previous versions and these increased the robustness of the algorithm.

Several validation studies on AXB have shown that the results of dose calculations from AXB were able to achieve comparable accuracy to MC methods¹⁰ or measurements in homogenous water medium^{8,16} and in heterogeneous media.^{7,9–15} Vassiliev et al.⁷ showed agreement within 2% between AXB and MC in a hetero-

geneous slab phantom as well as in a breast treatment plan on an anthropomorphic phantom. Bush et al.⁹ investigated the dosimetric accuracy of AXB with MC methods for 6 and 18 MV photon beam incident on homogenous and heterogeneous geometries, and compared the results against AAA. That study reported better agreement between MC and AXB ($\pm 3.0\%$) than between MC and AAA (up to 17.5%). Fogliata et al.¹⁰ investigated AXB in heterogeneous virtual phantoms characterized by simple geometry structures and then compared against MC and AAA. The results from that study showed that the calculated dose distributions between AXB and MC had good agreement at 6 and 15 MV photon beam. Han et al.^{12,13} reported better accuracy of AXB results when compared to the measurements in the Radiological Physics Center (RPC) head and neck phantom and chest phantom. Kan et al.¹⁴ showed that AAA overestimated the doses by up to 10%, while the measured doses matched those of AXB to within 3% near air/tissue interfaces in the anthropomorphic phantom. Yan et al.¹⁵ demonstrated that AAA overestimated doses by up to 8.96% close to the lung/solid water interface, while AXB reduced that to 1.64%.

2. Aim

This study is collocated in this scenario where several investigations on AXB have been carried out, analysing AXB in comparison with MC simulations. The works of cited authors are focused on clinical regions such the lung and head/neck, where free air can be an issue in dose calculation for type A and B algorithms. Nevertheless, a clinical region often presents structures with different densities (as bone, muscle and water or fat) and sometimes also a pocket air is present. Head/neck and abdomen are two examples of clinical regions where free air and variable density structures are present, where radiation interactions are not well modelled by pencil beam based algorithms.

The novel aspect of this study is to compare AXB dose-to-medium calculation, AAA dose calculation and absolute dose GafChromic film measurements where different density structures and air gaps are present. Fogliata et al.¹⁰ reported that AXB dose-to-water calculation shows strong differences compared with Monte Carlo calculations in regions with heterogeneities. The aim of this work is the implementation of AXB in clinical practice in the radiotherapy department of the authors. AXB dose-to-water use is not recommended in this scenario, so only AXB dose-to-medium is taken in consideration.

3. Material and methods

3.1. Homogeneous unit density phantom

There are two steps in the validation of a calculation algorithm. The first step is to validate the algorithm with homogenous phantoms and regular fields. The purpose of the tests in a homogeneous phantom is to provide a fundamental validation of AXB against measurements in water. In this step the materials used are two dimensional measurements of dose profile, acquired earlier in the year by clinical physicists with MapCheck diode array during the commissioning of the TrueBeam treatment units, and the gamma analysis^{3,4} performed by the author of this work with SNC Patient. To analyse the results, the recommendations of the Netherlands Commission of Radiation Dosimetry (NCD) report number 15¹ were followed. The recommended tolerance levels for the accuracy of photon beam dose calculations in the presence of uniform beams are: Global Gamma Criteria, 2%/2 mm, 10% Threshold, and expected pass rate of 95%. With more complex fields, in the presence of wedge and asymmetric fields, NCD allows increasing the tolerance to 3%/2 mm. Dose calculations using AXB, reported as dose to

medium, were made in a homogeneous phantom with density 1.0 g cm^{-3} , the outer dimension of $30 \times 30 \times 25 \text{ cm}^3$ for the following fields:

- 5 square fields from 4×4 to $22 \times 22 \text{ cm}^2$,
- 2 rectangular fields, 5×22 and $22 \times 5 \text{ cm}^2$.
- 6 wedged fields from 6×6 to $20 \times 20 \text{ cm}^2$, with 45 degrees and 60 degrees;
- 3 asymmetric fields
 - Asymmetric 1 [x1: -10, x2: 10, y1: 0, y2: 10],
 - Asymmetric 3 [x1: 0, x2: 10, y1: -10, y2: 10],
 - Asymmetric 4 [x1: -10, x2: 0, y1: -10, y2: 10]
- asymmetric wedged fields, with 45 degrees and 60 degrees;
 - Asymmetric 2 EDW45IN [x1: -10, x2: 10, y1: -10, y2: 0]
 - Asymmetric 4 EDW60IN [x1: 0, x2: 10, y1: -10, y2: 10]
 - Asymmetric 5 EDW60OUT [x1: -10, x2: 10, y1: 0, y2: 10]
 - Asymmetric 6 EDW45OUT [x1: -10, x2: 10, y1: -10, y2: 0]
- fields shaped with multi leaf collimator (MLC) taken from the NCD report: see **Appendix A**.

Dose calculation using the AXB algorithm was performed with a dose grid resolution of $1 \times 1 \times 1 \text{ cm}^3$ for all fields, except for $22 \times 22 \text{ cm}^2$ that was performed with a dose grid resolution of $2.5 \times 2.5 \times 2.5 \text{ cm}^3$. MapCheck was used in combination with Water Equivalent Phantoms (WEP) to evaluate the beam at various depths, i.e. 2 cm (without WEP), 10 cm and 20 cm. WEPs are free of cavities and other flaws and are not affected by temperature changes. The phantom scatters and attenuates diagnostic and radiotherapy range x-rays in the same way as water. They can also be used for relative ionization, depth dose measurements along with the proton and electron beam calibrations.

The source size for AAA 6X in beam configuration is $1 \times 1 \text{ mm}$ and AXB spot/source size is $0 \times 0 \text{ mm}$. The source size in beam configuration is not a true measure of the incident spot size on the target but a factor recommended by Varian. Measurements of the spot size have been performed using small fields $1 \times 1 \text{ cm}$ and $2 \times 2 \text{ cm}$ at two depths 5 cm, 10 cm deep in a water tank, using a diode detector. Measured profiles for each of these fields at both depths have been compared to the planning system generated profiles for a range of spot sizes, varying both X and Y to get the best agreement, using a gamma analysis.

3.2. Heterogeneous interfaces phantoms “P1” and “P2”

The second step in the validation of a calculation algorithm is to validate the algorithm in presence of heterogeneities. For this purpose two phantoms have been created. The first phantom simulated an air gap in tissue and the other simulated the abdominal region. The surface of both phantoms was 90 cm SSD, 250 MU were delivered. Two GafChromic EBT2 films were positioned one above and one below air gap, 5 mm from the gap (see Fig. 1). This position was chosen for two reasons: (i) to avoid deep dose gradient regions brought by the loss of backscatter from the air or from rebuild up in the water slab, where a minor positional error could lead to a large dose difference, and (ii) to evaluate algorithm predictions in clinical regions. The films were irradiated with a 6 MV photon beam for small and large fields.

The author of this work modelled the phantoms in Eclipse and calculated the dose deposition for both phantoms using AXB and AAA algorithms. The first phantom (P1 in the following), simulates the head/neck region and it is composed of a pocket air gap of 30 mm and two homogenous water equivalent slabs of 55 mm of thickness each. The material surrounding the air gap (mass density $0.00151 \text{ g cm}^{-3}$, -1000 HU) was assigned a mass density of 1.0 g cm^{-3} (-3 HU) corresponding to water in the AXB 13.7 material table.

The phantom was irradiated by a beam of $3 \times 3 \text{ cm}^2$ field, which is a standard size for a small beam, and by a beam of $10 \times 10 \text{ cm}^2$.

The second phantom (P2 in the following) simulates the abdominal region. It was created in order to simulate the area in the rectum, or bowel. P2 is composed of a pocket air gap surrounded by water, muscle and bone slabs. The algorithm assigned automatically a density of 1.0 g cm^{-3} for water (-3 HU), 1.85 g cm^{-3} and 1.05 g cm^{-3} for the bone and muscle. However when the mass density for the bone and muscle were measured, the values of 1.56 g cm^{-3} (896 HU) and 1.07 g cm^{-3} (53 HU), respectively, were obtained. These values were assigned to the phantom for the dose calculations.

Also in this case the films are positioned in a clinical region, 5 mm from the pocket air in order to avoid deep dose gradient regions. Film 1 is positioned above the air gap and film 2 is below the air gap (see Fig. 2).

The phantom was irradiated by a beam of $5 \times 5 \text{ cm}^2$ field, which represent a clinical field size.

GafChromic films [GafChromic® EBT2, International Specialty Products (ISP), NJ] are used for absolute dose measurements. The films were positioned between two water equivalent slabs, at a

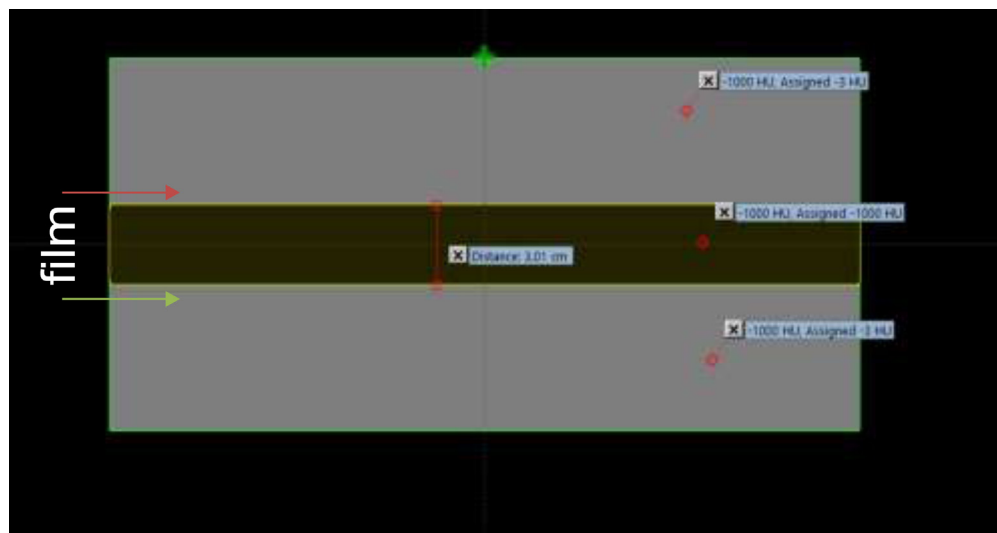


Fig. 1. Heterogeneous interface phantom P1. Locations of GafChromic EBT2 films are indicated. Water equivalent slab is assigned a density of 1 g cm^{-3} . Air density assigned is $0.00151 \text{ g cm}^{-3}$.

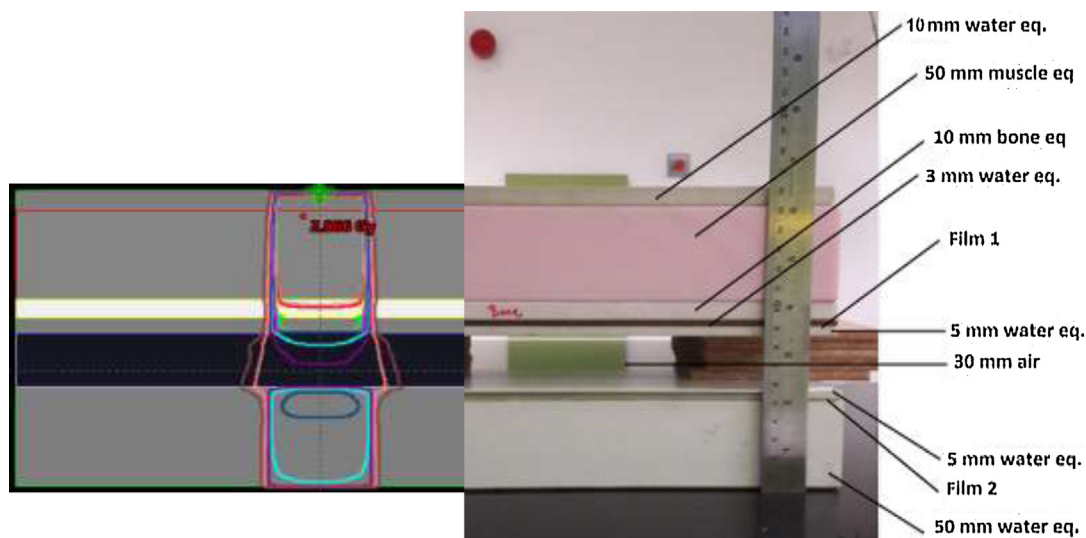


Fig. 2. Dose distribution for a field $5 \times 5 \text{ cm}^2$, 6 MV, 90 SSD, 250MU predicted by AXB (on the left) and deposited in a heterogeneous interface phantom “P2” (on the right). Locations of Gafchromic EBT2 films are indicated. Water, muscle and bone slabs are assigned a density of 1 g cm^{-3} , 1.07 g cm^{-3} and 1.56 g cm^{-3} , respectively. Air density assigned is $0.00151 \text{ g cm}^{-3}$.

distance of 5 mm from the interfaces of different densities slabs. There are several benefits to the use of GafChromic films for dose evaluation:

- Films are self-developing in real time and generate optical density response to ionisation radiation. This optical density can be easily scanned and measured by a software;
- measurements by FilmQA Pro Software can be performed several times also weeks after the exposure;
- Films are tissue equivalent,^{19,21} the dose absorbed by the film, with the right calibration, gives the dose absorbed by tissue;
- Films can be handled in environmental light, but they are sensitive to ultraviolet light²¹
- Films can be easily cut into the required shape
- Films can be cleaned with water, in order to remove artefacts from the scanned images

Radiochromic film consists of an ultrathin ($\sim 28 \mu\text{m}$ thick) radiosensitive layer, sandwiched symmetrically between two polyester layers ($100 \mu\text{m}$ thick). Exposure of a radiochromic film to ionising radiation causes a polymerisation in the crystal of the active layer. Care must be taken in the scanning of films because the optical density is a strong function of the film orientation.¹⁹ Lynch et al.¹⁹ recommend using only the central portion of the scanner bed where lamp variation is the smallest. Following these suggestions, a unique film was cut in several parts of the same size. The top right corner of each piece film was marked and, during the scan, the orientation of each piece was kept the same. The films were scanned and analysed using the FilmQA Pro procedure recommended by AshlandTM.²⁰ Seven films were irradiated in a field $10 \times 10 \text{ cm}^2$, at a depth of 5 cm WEP to an increasing known dose. These films, along with a non-irradiated film, were used to obtain the calibration curve. Two test films were irradiated with a known dose in calibration conditions to check the correctness of the calibration curve.

3.3. Sources of uncertainty

There are several sources of uncertainty in this study, for example the slabs thickness ($\pm 0.1 \text{ mm}$), the SSD ($\pm 1 \text{ mm}$), the field size ($\pm 1 \text{ mm}$), the position of dose point taken from Eclipse ($\pm 1 \text{ mm}$)

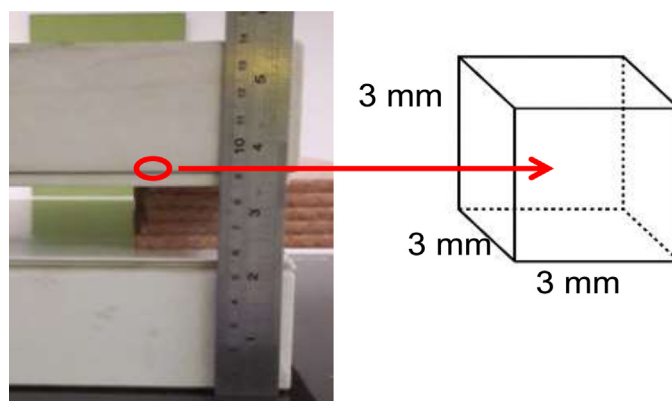


Fig. 3. Virtual cube of $3 \text{ mm} \times 3 \text{ mm} \times 3 \text{ mm}$ where average and standard deviation of dose predicted by AAA and AXB were calculated.

and various contributes to the film noise, as scan Gaussian noise and calibration curve uncertainties. Due to all these uncertainties, the dose obtained from Eclipse was not taken at a single point but in a volume centred on the beam axis at the expected depth of film. The average and standard deviation of dose predicted by AAA and AXB were calculated in a virtual cube of $3 \text{ mm} \times 3 \text{ mm} \times 3 \text{ mm}$ (see Fig. 3).

The difference between the dose measured by the film and the dose predicted by the algorithms is defined as:

$$D = \frac{(AXB|Dose - Film_{Dose})}{Film_{Dose}}$$

and the related uncertainties.²²

4. Results

4.1. Homogeneous interfaces phantom

Table 1 summarises the results obtained from the gamma analysis for the homogenous phantom and regular fields. The table with individual pass rates for each field is reported in Appendix B.

At 80 cm and 90 cm SSD the table shows:

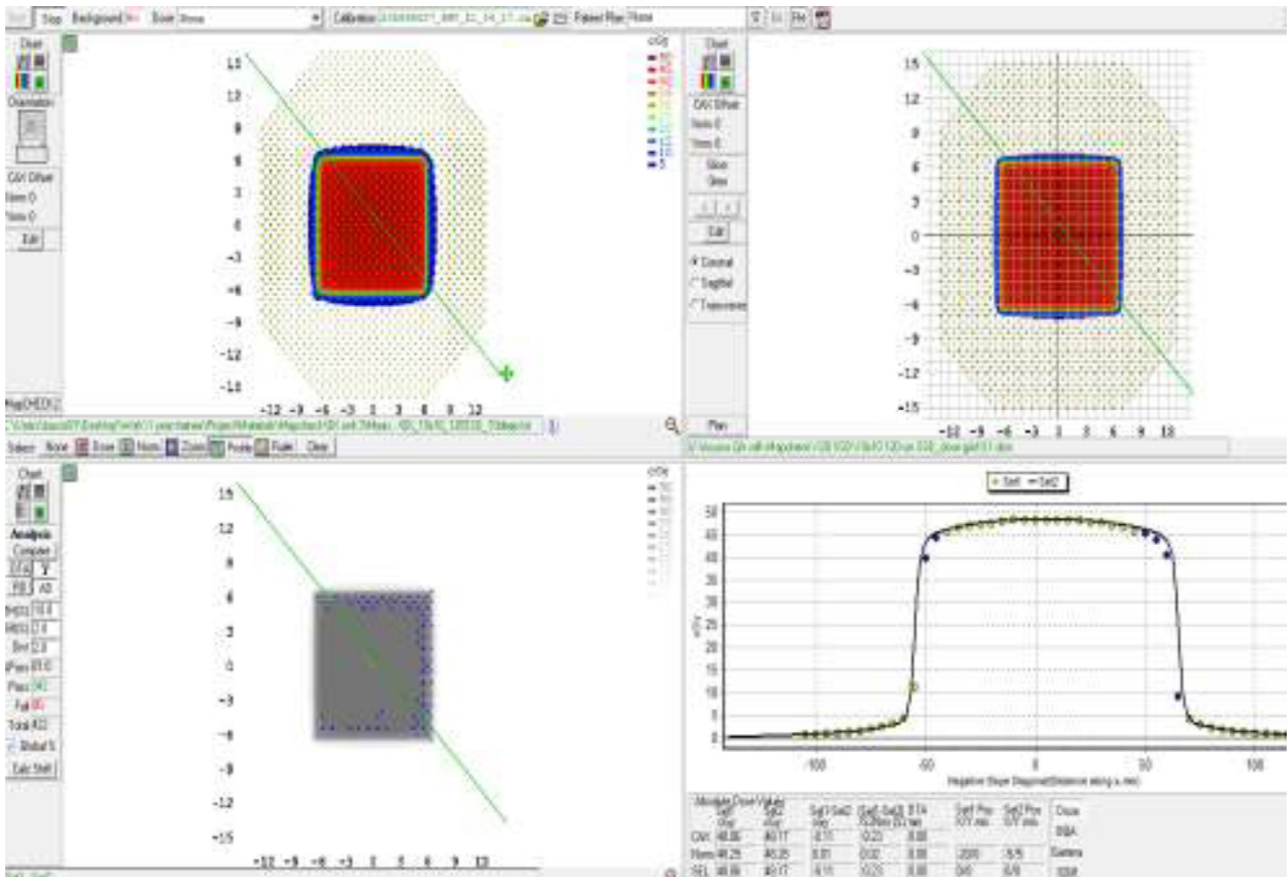


Fig. 4. Results of gamma analysis with global gamma criteria, 2%/2 mm, 10% Threshold. MapCheck was irradiated at 120 cm SSD, 10 cm WEP with 10 × 10 cm² field.

Table 1

Results for the homogenous interface phantom with regular fields obtained from measurements on Varian TrueBeam. The table shows the minimum pass rate, the pass rates lower than 95% are highlighted in bold font. Regular fields are: 4 × 4 cm², 5 × 5 cm², 10 × 10 cm², 15 × 15 cm² and 22 × 22 cm². Wedged fields are: 6 × 6 cm² 45°IN, 10 × 10 cm² 45°OUT, 10 × 10 cm² 60°IN, 10 × 10 cm² 60°OUT, 20 × 20 cm² 60°OUT.

	SSD 90 cm			SSD 80cm		SSD 100 cm		SSD 120 cm	
	2 cm	10 cm	20cm	2 cm	10 cm	2 cm	10 cm	2 cm	10 cm
Regular fields	100%	98%	96%	100%	95.3%	99.6%	95%	98.2%	81%
5 × 22	98.2%	91.1%	94.4%			99.60%	84.1%	96.60%	76.8%
22 × 5	99.6%	100%							
Wedged	99.6%	98.7%		100%	98%	99.50%	95.2%		
Asymmetric	98%	95.6%	98.30%						
MLC	95.6%	97.8%	95.60%	100%	99.5%	100%	95.80%		

- For regular fields a high pass rate (>96%), but for the 5 × 22 cm² field a higher dose difference criteria of 3% was required.
- For wedged fields, asymmetric fields and MLC a good pass rate (>95%) without any shift.

At 100 cm and 120 cm SSD the table shows:

- For regular fields a high pass rate (>96%) at a depth of 2 cm and a lower pass rate (min 76%) with WEP of 10 cm. In this case the shape of beam measured is narrower than that calculated by AXB.
- For wedged fields and MLC fields good pass rate (>95%).

In general, the pass rate obtained is high (>95%), with some exceptions. For example, the 5 × 22 cm² field has the lower pass rate across the whole SSD range. This field shows the minimum pass rate of 76.8% at 120 cm SSD and 10 cm WEP. When analysing all the results at 120 cm SSD, it can be noticed that also the regular fields have a lower pass rate with 10 cm WEP (81%). This is com-

parable with what is obtained during the commissioning of AAA (85.6%). The dose calculated by the algorithm is higher than the dose measured by MapCheck (see Fig. 4) with a prevalence of low points on the boundaries of the field.

4.2. Heterogeneous interfaces phantoms “P1” and “P2”

Fig. 5 shows the dose deposition predicted by AXB and AAA calculated along the central axis of 3 × 3 cm² and 10 × 10 cm² fields in phantom P1. AAA handles the heterogeneities as a density based correction applied to dose kernels calculated in water and the profile of the predicted dose is smooth. In turn, AXB takes into consideration the chemical composition of materials and explicitly models the physical interaction of radiation with matter. For this reason, the dose profile of AXB is different from AAA: near the pocket air surface the dose drops due to the lack of photon backscatter from the air. After the pocket air, a re-build up region in the water slab is well predicted by AXB.

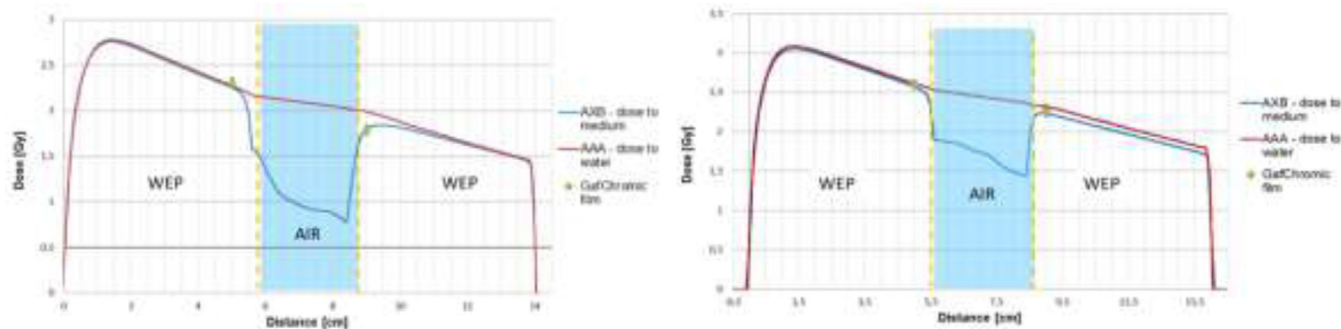


Fig. 5. Dose deposition predicted by AXB and AAA calculated along the central axis for a beam of $3 \times 3 \text{ cm}^2$ (on the left) and $10 \times 10 \text{ cm}^2$ (on the right) incident in P1. Note the differences in the dose deposition in the air pocket region due to the different calculation algorithms: AAA handles the heterogeneities as density based correction while AXB models the physical interaction of radiation with matter. For this reason, the dose deposition of AAA is smoother than AXB. The location of the GafChromic films in the phantoms and the absolute dose measurement are shown in the graph by the green points. In the region before the air gap AXB, AAA and films are in agreement within 3%. On the region below the air gap, in the $3 \times 3 \text{ cm}^2$ beam, AXB shows a difference with films of 0.2% while AAA shows a difference of 11.2% on the same point. In the $10 \times 10 \text{ cm}^2$ beam, in the region below the air, AXB and AAA show a similar difference with films: 1.9% (AXB) and 1.8% (AAA).

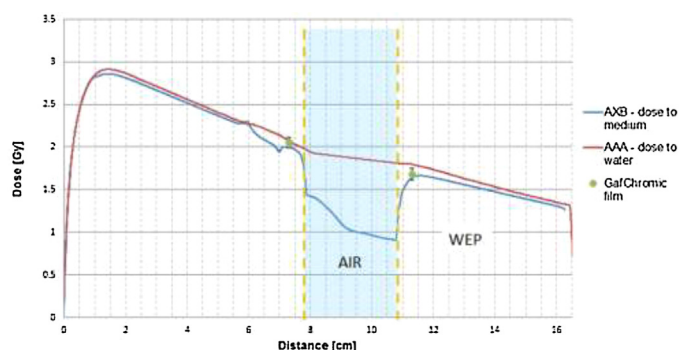


Fig. 6. Dose deposition predicted by AXB and AAA calculated along the central axis for a beam of $5 \times 5 \text{ cm}^2$ incident in P2. Note the AXB profile shows: the increase backscatter passing through water/bone and the loss of backscatter passing through bone/water and water/air. Also visible is the re-build up in the water slabs above and below the air pocket. The positions of the GafChromic films on the phantom and the measurements in absolute dose are shown by the green points.

In the region before the air gap AXB, AAA and films are in agreement within 3%. On the region below the air gap, in $3 \times 3 \text{ cm}^2$ beam, AXB shows a difference with films of 2.94% while AAA shows a difference of 6.9% on the same point.

Fig. 6 shows the comparison of dose deposition predicted by AAA and AXB calculated on the central axis for 6 MV, $5 \times 5 \text{ cm}^2$, 90 cm SSD, 250MU beam that interacts with P2. The location of films is visible in the graph by the green points. The film before the air gap is used to check the setup and a very good agreement would be expected in this region. AXB profile shows:

- an increase in dose between water and the bone created by backscatter from the bone
- a drop of dose between the bone and water created by a lack of backscatter from water; this can be explained by the increase attenuation and Compton scattering in the bone slab due to the increased density of the bone slab
- a little re-build up on the water slab followed suddenly by a drop of dose created by a lack of backscatter from the air pocket
- a re-build up in the last slab of water.

In Table 2 the results of AXB and films dose measurements are reported. The uncertainties in the dose calculated with AXB range from 0.3% to 1.8%, and for the film from 1.9% to 4.3% of dose. The AXB calculations were within 3% of dose measured by films, as predicted by literature.⁸ Table 3 reports the results between AAA and films dose. The uncertainties of dose calculated with AAA range from 0.1% to 0.9% of dose. The AAA calculations were within 2% of dose

measured by films above the air gap but below the air gap AAA overestimated doses by up to 11%.

5. Discussion

In this work the dose calculated by AXB for a 6 MV beam is compared with the dose measured by MapCheck in a water phantom, GafChromic films in the presence of heterogeneities and the dose calculated by AAA. The goal of this work is to understand better the limitations and strengths of the AXB algorithm. In the WEP phantom, with fields of increased complexity, AXB shows a good agreement with the MapCheck measurement, in line with the tolerances suggested by the Netherlands Commission of Radiation Dosimetry. However, AXB shows an incorrect calculation of the beam penumbra at 120 cm SSD. This is more visible with increasing depth both for square and long rectangular fields (see Fig. 4 and 7). This field was chosen because extremities are typically treated at extended SSDs with long narrow fields.

In this case, the dose profile analysis shows that the profile measured is narrower than that calculated by AXB one. The position of gamma analysis fault points suggests that the incorrect calculation is probably due to an incorrect modelling of the penumbra by the algorithm and it is more visible in extreme cases, as at 120 cm SSD. The gradient in the penumbra is less steep than seen with the measurement. Therefore, for long narrow fields at extended SSD the actual coverage may be less than the calculated coverage. In the clinical context, this result suggests that one should be careful to check the coverage of a target positioned in depth, with an SSD of 120 cm, because the dose calculated at the target boundaries is greater than the actual one. This can affect the correctness of target dose calculation and, in this situations, it could be reasonable to increase the target volume.

When analysing the results obtained at 80 cm and 90 cm SSD, a high pass rate can be noticed in this range which is more used during radiotherapy treatments. The results of gamma analysis show at 90 cm SSD a low pass rate (91.1%) for the narrow field with 10 cm WEP, but the maximum % dose difference for fault gamma is 2.5%. We conclude that the fault is not severe and we are confident that the algorithm calculates the dose properly at 90 cm.

In the presence of heterogeneities the dose calculated by AXB is less than 3% different from GafChromic films measurements, as predicted by literature.⁸ Instead, AAA overestimates the dose by up to 11%, as seen in P1 with the $3 \times 3 \text{ cm}^2$ field. The algorithm corrects

Table 2
AXB and film dose measurements for a beam of 6 MV, 250MU, SSD = 90 cm incident in P1 and P2.

P1–3 × 3 cm ² field			
Film position	Dose AXB (cGy)	Dose Film (cGy)	Difference (%)
Above air (50 mm)	225 ± 2	230 ± 5	–2.20 ± 2.4
Below air (90 mm)	179 ± 3	179 ± 6	+0.2 ± 3.9
P1–10 × 10 cm ² field			
Film position	Dose AXB (cGy)	Dose Film (cGy)	Difference (%)
Above air (50 mm)	257 ± 2	260 ± 5	–1.3 ± 2.2
Below air (90 mm)	223 ± 1	227 ± 7	–1.9 ± 2.0
P2–5 × 5 cm ² field			
Film position	Dose AXB (cGy)	Dose Film (cGy)	Difference (%)
Above air (73 mm)	199 ± 1	205 ± 6	–2.70 ± 3.3
Below air (113 mm)	163 ± 2	167 ± 7	–2.94 ± 4.8

Table 3
AAA and film dose measurements for a beam of 6 MV, 250MU, SSD = 90 cm incident in P1 and P2.

P1–3 × 3 cm ² field			
Film position	Dose AAA (cGy)	Dose Film (cGy)	Difference (%)
Above air (50 mm)	227 ± 2	230 ± 5	–1.6 ± 2.3
Below air (90 mm)	199 ± 1	179 ± 6	+11.2 ± 6.3
P1–10 × 10 cm ² field			
Film position	Dose AAA (cGy)	Dose Film (cGy)	Difference (%)
Above air (50 mm)	261 ± 1	260 ± 5	+0.3 ± 2.1
Below air (90 mm)	231 ± 1	227 ± 7	+1.8 ± 3.2
P2–5 × 5 cm ² field			
Film position	Dose AAA (cGy)	Dose Film (cGy)	Difference (%)
Above air (73 mm)	207 ± 2	205 ± 6	+1.1 ± 3.3
Below air (113 mm)	179 ± 1	167 ± 7	+6.9 ± 5.8

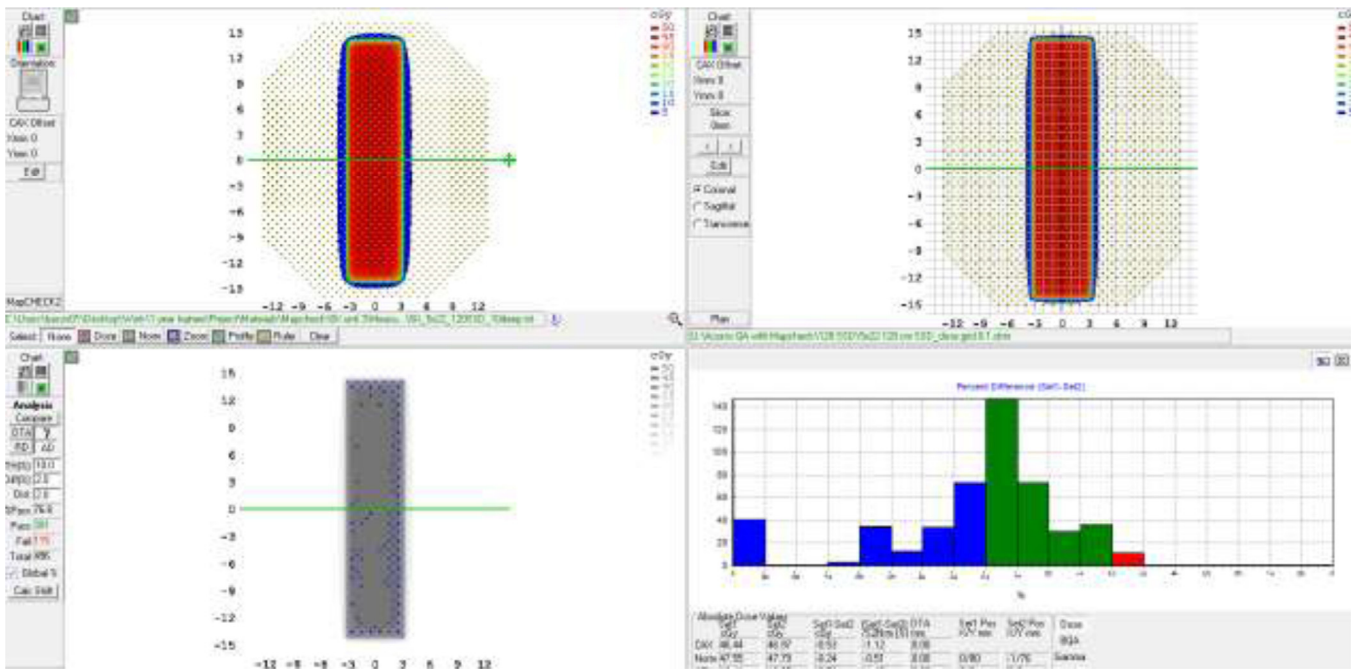


Fig. 7. Results of gamma analysis with global gamma criteria, 2%/2 mm, 10% Threshold. MapCheck was irradiated at 120 cm SSD, 10 cm WEP with 5 × 22 cm² field.

the heterogeneities, scaling the absorbed energy of photon scatter kernels calculated in water $K\beta(x,y,z)$ by density of heterogeneity and it doesn't take into consideration the physical interaction of radiation with matter.^{17,18} AXB takes in consideration the chemical composition of materials and explicitly models the physical interaction of radiation with matter. If we compare the dose distribution in P1 for a beam 6 MV, 10 × 10 cm², 90 cm SSD, calculated by AAA and AXB, we notice some differences in the air gap region: AXB takes in consideration also the interactions of beam with air (see Fig. 8).

Energy that is released at the centre of the beam is spread laterally by electrons that have an increased range in the low density material.^{17,18} The beam edge is blurred in low-density absorbers due to the increased lateral motion of charged particles and the lack of electron equilibrium (lateral loss of Transient Charged Particle Equilibrium, TCPE) at the field edge. The result is that penumbra increases in the pocket air region. AAA does not take into consideration the interaction of beam with air and the lateral spread of the beam is not visible because the air gap is modelled as a thin slab of water.

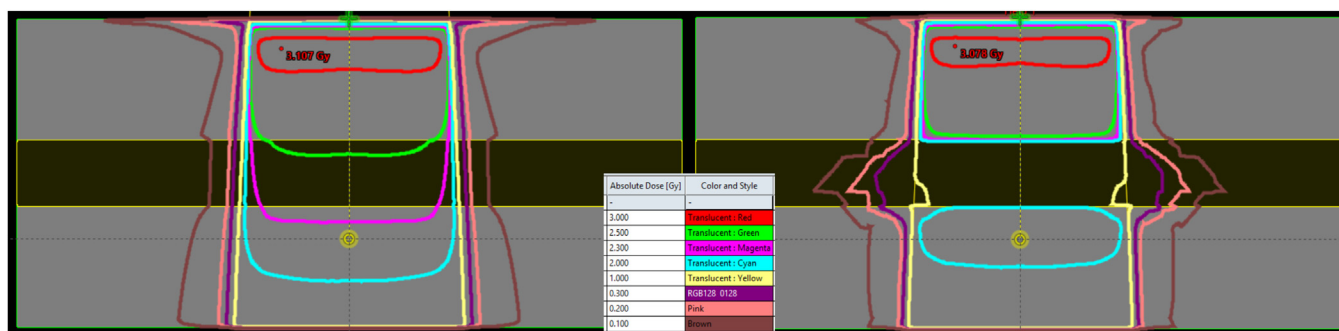


Fig. 8. Dose distribution for a beam 6 MV, $10 \times 10 \text{ cm}^2$, 90 cm SSD, calculated by AAA (on the left) and AXB (on the right) incident in air pocket phantom P1. Note the dose reduction in the air region and the penumbral flaring of the beam predicted by AXB. Absolute dose isolevels are the same.

6. Conclusion

On the oncologic radiotherapy department where the authors developed this work, AXB is in clinical use for lung SABR planning but has not yet been validated for VMAT planning. AAA is the clinical dose calculation algorithm used for all the other non-SABR techniques. The aim of this work was to validate the AXB algorithm and determine if it is suitable for VMAT planning, in order to introduce it clinically on the department. The results of this work derive from absolute dose measurements, not from simulations and they are in line with literature. AXB meets the tolerance levels suggested by NCD.¹

Nevertheless, this work highlights also the weakness of type B algorithms in the presence of free air. The results of absolute dose measurements performed with GafChromic EBT in the heterogeneous phantom, simulating the abdominal region, prove that the dose differences after the air calculated by AXB are less than 3% while with AAA differences up to 11% can be obtained. The results of this work lead to the conclusion that type B algorithms are less accurate for dose calculation in the presence of free air.

In our opinion, analysing the results of this study, AXB is suitable to use clinically in complex clinical regions where different density structures and free air gaps occur (as head/neck region in the sinus cavities and airways). The AXB algorithm can replace AAA in Eclipse for standard VMAT planning. In this way, the algorithm will bring a more accurate dose calculation not only in head/neck plans but also the abdominal plans will benefit. Moving from AAA to AXB, the coverage in areas adjacent to air gaps will differ. AAA currently shows smoothly changing isodoses in heterogeneous areas while AXB shows a deep gradient of dose after the air gap.

In conclusion, the substitution of AAA with AXB in Eclipse will bring benefits not only to head/neck treatment but also to regions such as abdomen.

Funding

None.

Conflict of interest

None.

Financial disclosure

None.

Ethical approval

Not required.

Appendix A. Supplementary data

Supplementary material related to this article can be found, in the online version, at doi:<https://doi.org/10.1016/j.rpor.2020.03.018>.

References

- Netherlands Commission on Radiation Dosimetry, Report 15, "Quality assurance of 3-D treatment planning systems for external photon and electron beams", March 2005.
- ICRU Report 83, Journal of the ICRU 10 1 (2010), Oxford University Press, doi:10.1093/jicru/ndq001.
- Low D, Dempsey J. Evaluation of the gamma dose distribution comparison method. *Med Phys.* 2003;30(9):2455–2464.
- Low Daniel A, Moran Jean M, Dempsey James F, Dong Lei, Oldham Mark. Dosimetry tools and techniques for IMRT. *Med Phys.* 2011;38(3):1313. <http://dx.doi.org/10.1118/1.3514120>.
- Ahnesjo Anders, Aspradakis Maria Mania. Dose calculations for external photon beams in radiotherapy, TOPICAL REVIEW. *Phys Med Biol.* 1999;44:R99–R155.
- Hasenbalg F, Neuenschwander H, Mini R, Born E. Collapsed cone and analytical anisotropic algorithm dose calculation compared to VMC++ Monte Carlo simulations in clinical cases. *J Phys Conf Ser.* 2007;74:012007. <http://dx.doi.org/10.1088/1742-6596/74/1/012007>.
- Vassiliev ON, Wareing TA, McGhee J, Failla G, Salehpour MR, Mourtada F. Validation of a new grid based Blotzmann equation solver for dose calculation in radiotherapy with photon beams. *Phys Med Biol.* 2010;55:581–598 [PubMed: 20057008].
- Fogliata A, Nicolini G, Clivio A, Vanetti E, Mancosu P, Cozzi L. Dosimetric validation of Acuros XB Advanced Dose Calculation algorithm: Fundamental characterization in water. *Phys Med Biol.*
- Bush K, Gagne IM, Zavgorodni S, Ansbacher W, Beckham W. Dosimetric validation of Acuros XB with Monte Carlo methods for photon dose calculations. *Med Phys.* 2011;38:2208–2221 [PubMed: 21626955].
- Fogliata A, et al. Dosimetric evaluation of Acuros XB Advanced Dose Calculation algorithm in heterogeneous media. *Radiat Oncol.* 2011. <http://dx.doi.org/10.1186/1748-717X-6-82>.
- Ojala J, Kapanen M, Sipilä P, Hyödynmaa S, Pitkänen M. The accuracy of Acuros XB algorithm for radiation beams traversing a metallic hip implant - comparison with measurements and Monte Carlo calculations. *J Appl Clin Med Phys.* 2014;15(5):162–176.
- Han T, Mourtada F, Kisling K, Mikell J, Followill D, Howell R. Experimental validation of deterministic Acuros XB algorithm for IMRT and VMAT dose calculations with the Radiological Physics Center's head and neck phantom. *Med Phys.* 2012;39:2193–2202 [PMCID: PMC3337663] [PubMed: 22482641].
- Han T, Followill D, Mikell J, et al. Dosimetric impact of Acuros XB deterministic radiation transport algorithm for heterogeneous dose calculation in lung cancer. *Med Phys.* 2013;40(5):051710 <https://www.ncbi.nlm.nih.gov/pubmed/23635258>.
- Kan MW, Leung LH, Yu PK. Verification and dosimetric impact of Acuros XB algorithm on intensity modulated stereotactic radiotherapy for locally persistent nasopharyngeal carcinoma. *Med Phys.* 2012;39:4705–4714 [PubMed: 22894395].
- Yan, et al. Clinical implementation and evaluation of the Acuros dose calculation algorithm. *J Appl Clin Med Phys.* 2017. <http://dx.doi.org/10.1002/acm2.12149>.
- Fogliata A, et al. On the dosimetric behaviour of photon dose calculation algorithms in the presence of simple geometric heterogeneities: comparison with Monte Carlo calculations. *Phys Med Biol.* 2007;52(5). IOP Publishing Ltd.
- Tissue inhomogeneity corrections for megavoltage photon beams, AAPM report n.85, TG 65, Medical Physics Publishing, August 2004.

18. True three-dimensional dose computations for megavoltage x-ray therapy: A role for the superposition principle. *Australas Phys Eng Sci Med.* 1992;15:159–178.
19. Lynch B, Kozelka J, Ranade M, Li J, Simon W, Dempsey J. Important considerations for radiochromic film dosimetry with flatbed CCD scanners and EBT GAFCHROMIC® film. *Med Phys.* 2006;33(12):4551–4556.
20. Gafchromic films calibration procedure using FilmQA™ Pro by Ashland™ can be found on the website: <http://www.gafchromic.com/filmqa-software/filmqapro/calibration.asp>.
21. Khan F. *Physics of radiation therapy*. Philadelphia: Wolters Kluwer Health.; 2010.
22. Hughes I, Hase T. *Measurements and their uncertainties*. Oxford: Oxford University Press; 2011.